THE JOURNAL OF BIOLOGICAL CHEMISTRY VOL. 286, NO. 31, pp. 27183–27196, August 5, 2011

Distal End of Carboxyl Terminus Is Not Essential for the Assembly of Rat Eag1 Potassium Channels*

Received for publication, March 3, 2011, and in revised form, June 5, 2011 Published, JBC Papers in Press, June 6, 2011, DOI 10.1074/jbc.M111.233825

I-Hsiu Chen[‡1], Jui-Hsiang Hu[‡1], Guey-Mei Jow[§], Chao-Chin Chuang[‡2], Ting-Ting Lee[‡2], Dai-Chi Liu[‡2], and Chung-Jiuan Jeng[‡3]

From the [‡]Institute of Anatomy and Cell Biology, School of Medicine, National Yang-Ming University, Taipei 12212 and the [§]School of Medicine, Fu-Jen Catholic University, Hsin-Chuang, Taipei County 24205, Taiwan

The assembly of four pore-forming α-subunits into tetramers is a prerequisite for the formation of functional K^+ channels. A short carboxyl assembly domain (CAD) in the distal end of the cytoplasmic carboxyl terminus has been implicated in the assembly of Eag α-subunits, a subfamily of the ether-à-go-go K^+ channel family. The precise role of CAD in the formation of Eag tetrameric channels, however, remains unclear. Moreover, it has not been determined whether other protein regions also contribute to the assembly of Eag subunits. We addressed these questions by studying the biophysical properties of a series of different rat Eag1 (rEag1) truncation mutants. Two truncation mutants without CAD (K848X and W823X) yielded functional phenotypes similar to those for wild-type (WT) rEag1 channels. Furthermore, nonfunctional rEag1 truncation mutants lacking the distal region of the carboxyl terminus displayed substantial dominant-negative effects on the functional expression of WT as well as K848X and W823X channels. Our co-immunoprecipitation studies further revealed that truncation mutants containing no CAD indeed displayed significant association with rEag1-WT subunits. Finally, surface biotinylation and protein glycosylation analyses demonstrated that progressive truncations of the carboxyl terminus resulted in aggravating disruptions of membrane trafficking and glycosylation of rEag1 proteins. Overall, our data suggest that the distal carboxyl terminus, including CAD, is dispensable for the assembly of rEag1 K^+ channels but may instead be essential for ensuring proper protein biosynthesis. We propose that the S6 segment and the proximal carboxyl terminus may constitute the principal subunit recognition site for the assembly of rEag1 channels.

Voltage-gated K^+ channels contribute to many neurophysiological functions in the nervous system, such as controlling neuronal excitability, setting neuronal firing frequencies, shaping action potential waveforms, and modulating neurotransmitter release (1). A functional voltage-gated K^+ channel includes four pore-forming α-subunits (2). The formation of tetrameric K^+ channels requires specific inter-subunit associations via the assembly domain located within individual α-subunits. In Shaker-related (Kv1) channels, for example, the cytoplasmic amino-terminal tetramerization domain plays an important role in subunit tetramerization and subfamily-specific assembly (3–5). By contrast, in KCNQ (Kv7) channels, subtype-specific assembly has been shown to be determined by a coiled-coil domain in the distal carboxyl-terminal region (6–8).

The ether-à-go-go K^+ channel family encompasses three subfamilies as follows: Eag, Erg, and Elk (9). Quite similar to cyclic nucleotide-gated and hyperpolarization-activated cyclic nucleotide-modulated (HCN)[4] channels, one of the structural hallmarks of the ether-à-go-go K^+ channel family is the presence of a putative cyclic nucleotide-binding domain (CNBD) in the carboxyl terminus (9, 10). Interestingly, the assembly domain of Eag α-subunits has been ascribed to a 41-amino acid (Ala^{897}–Ser^{937}) carboxyl assembly domain (CAD) in the distal end of the carboxyl terminus (11). Moreover, CAD has been suggested to have a high probability of forming coiled-coil structure and is thus also called a tetramerizing coiled-coil (TCC) domain (12). Carboxyl-terminal assembly domains have been identified as well in other members of the CNBD-containing channel superfamily, including Erg channels, cyclic nucleotide-gated channels, HCN channels, and plant K^+ channels (AKT1 and KAT1) (10, 13–16).

The precise role of CAD in the formation of Eag tetrameric channels, however, remains unclear. Presumably, via coiled-coil interactions, CAD may serve as an association domain to drive tetramerization of Eag subunits (12). Yet, because CAD is less than 30 residues away from the very end of the protein, it is still unknown how a domain that is translated relatively late can effectively govern the assembly process. Furthermore, it is not obvious whether CAD functions as a recognition or stabilization motif. Most importantly, is CAD the sole and/or principal assembly domain for Eag channels? Subunit interaction sites for Erg channels, for instance, may involve both the amino and carboxyl termini (12, 16–18). Furthermore, in AKT1 and KAT1 plant K^+ channels, at least two distinct carboxyl-terminal domains have been implicated in subunit assembly (13, 14). It is therefore likely that other protein regions also contribute to the assembly of Eag subunits.

* This work was supported by National Science Council, Taiwan, Research Grant NSC97-2320-B-010-020-MY3 and by Aim for the Top University Plan, Ministry of Education, Taiwan (to C. J. J.).

[1] Both authors contributed equally to this work.
[2] Present address: Dept. of Physiology, College of Medicine, National Taiwan University, Taipei 10051, Taiwan.
[3] To whom correspondence should be addressed. Tel.: 886-2-28267072; Fax: 886-2-28212884; E-mail: cjjeng@ym.edu.tw.

[4] The abbreviations used are: HCN, hyperpolarization-activated cyclic nucleotide-modulated; CAD, carboxyl assembly domain; CNBD, cyclic nucleotide-binding domain; Endo H, endoglycosidase H; HEK, human embryonic kidney; PNGase F, *N*-glycosidase F; rEag1, rat Eag1; Rolf, rat olfactory channel; TCC, tetramerizing coiled-coil; ANOVA, analysis of variance.

In this study, we aim to ascertain the structural basis of the assembly of Eag K^+ channels. By generating a series of different truncation mutants of rat Eag1 (rEag1) subunits, we have identified CAD-lacking truncation mutants that yielded functional phenotypes similar to those for wild-type (WT) rEag1 channels. Our biophysical studies further demonstrated that nonfunctional rEag1 truncation mutants lacking the distal region of the carboxyl terminus displayed substantial dominant-negative effects on the functional expression of rEag1-WT channels and that these truncation mutants can indeed be co-immunoprecipitated with rEag1-WT subunits. Our results suggest that CAD is not essential for the assembly of rEag1 K^+ channels.

EXPERIMENTAL PROCEDURES

Full-length and Truncated rEag1 Constructs—rEag1 cDNA subcloned into pcDNA3 was kindly provided by Dr. Olaf Pongs (Institute fur Neurale, Signalverarbeitung, Zentrum fur Molekulare Neurobiologie, Germany). Truncated rEag1 constructs that introduce a premature stop codon (denoted by X) at the site of mutation were generated by using QuickChange site-directed mutagenesis kit (Stratagene, La Jolla, CA), followed by DNA sequencing verification (Genome Research Center, National Yang-Ming University, Taiwan). For *in vitro* transcription, rEag1 cDNA was linearized with XbaI. Capped cRNA was transcribed *in vitro* from the linearized cDNA template with the mMessage mMachine T7 kit (Ambion, Austin, TX). Concentration of cRNA was determined by gel electrophoresis and verified with spectrophotometry (GeneQuant *Pro* RNA/DNA Calculator, Amersham Biosciences). To create epitope-tagged constructs for the mammalian expression system, rEag1 cDNA was subcloned into either pcDNA3.1-myc (Invitrogen) or pEGFP (Clontech).

cRNA Injection and Two-electrode Voltage Clamp Recording in Xenopus Oocytes—Adult female *Xenopus laevis* frogs (African *Xenopus* Facility, Knysna, South Africa) were anesthetized by immersion in Tricaine (1.5 g/liter). All animals were handled in accordance with the National Institute of Health Guide for the Care and Use of Laboratory Animals (NIH Publications No. 80-23, revised 1996). All procedures involving animals were performed in conformity with the animal protocol approved by the Lab Animal Council, National Yang-Ming University. Ovarian follicles were removed from *Xenopus* frogs, cut into small pieces, and incubated in ND96 solution ((in mM) 96 NaCl, 2 KCl, 1.8 $MgCl_2$, 1.8 $CaCl_2$, and 5 HEPES, pH 7.5). To remove the follicular membrane, *Xenopus* oocytes were incubated in Ca^{2+}-free ND96 containing collagenase (2 mg/ml) on an orbital shaker (~200 rpm) for about 60–90 min at room temperature. After several washes with collagenase-free, Ca^{2+}-free ND96, oocytes were transferred to ND96. Stage V–VI oocytes were then selected for cRNA injection. For all cRNA injection paradigms, the total volume of injection was always 41.4 nl per oocyte. To examine the phenotype of various rEag1 truncation mutants, about 80 ng of cRNA was injected into an oocyte. For co-expression experiments, it was imperative to find a submaximal cRNA concentration for rEag1-WT channels that will allow us to add an extra amount of mutant cRNA. Therefore, we empirically set up a fixed concentration of cRNA for injection, known as the standard cRNA mixture, in which the final injection amount for rEag1-WT cRNA was about 5 ng per oocyte. Injected oocytes were stored at 16 °C in ND96 solution supplemented with 50 mg/liter gentamycin. 2–4 days after cRNA injection, oocytes were functionally assayed in a recording bath containing Ringer solution ((in mM): 115 NaCl, 3 KCl, 1.8 $CaCl_2$, 10 HEPES, pH 7.2). Where indicated, 60 mM KCl was employed (by replacing NaCl) to record tail currents. Niflumic acid (0.5 mM) was added to the bath to minimize the contribution of endogenous Ca^{2+}-activated Cl^- currents. The bath volume was about ~200 μl. An agarose bridge was used to connect the bath solution with a ground chamber (containing 3 M KCl) into which two ground electrodes were inserted. Borosilicate electrodes (0.1–1 megohms) used in voltage recording and current injection were filled with 3 M KCl. K^+ currents through rEag1 channels were acquired, using the conventional two-electrode voltage clamp technique with an OC-725C oocyte clamp (Warner, Hamden, CT). Data were filtered at 1 kHz (OC-725C oocyte clamp) and digitized at 100 μs per point (10 kHz) by using the Digidata 1332A/pCLAMP 8.2 data acquisition system (Molecular Devices, Sunnyvale, CA). The holding potential was set at −90 mV. Passive membrane properties were compensated using the −P/4 leak subtraction method provided by the pCLAMP 8.2 software. All recordings were performed at room temperature (20–22 °C). Data analyses were performed via built-in analytical functions of the pCLAMP 8.2 software. To study steady-state voltage-dependent activation of channels, isochronal tail currents at −90 mV were normalized to the maximum amplitude to obtain the fraction of open channels (P_o) at the test potential (V). Data points were fit with a Boltzmann equation as follows: $P_o(V) = 1/\{1 + \exp((V_{0.5} - V)/k)\}$, where $V_{0.5}$ is the half-maximal voltage for activation, and k the slope factor of the P_o-V curve.

For co-expression experiments, one copy of the cRNA for a truncation mutant was added to the standard cRNA mixture (WT + H_2O) for oocyte injections, resulting in 1:1 molar ratio of WT and mutant. As a control, one copy of the WT cRNA was also added to the standard cRNA mixture for oocyte injections (WT + WT). The steady-state +60-mV current amplitude measured from each *Xenopus* oocyte co-expressing rEag1-WT and truncation mutant was normalized by the corresponding mean +60-mV K^+ current amplitude of rEag1-WT channels (WT + H_2O) measured from the same batch of oocytes on the same day of experiment, *i.e.* the mean +60-mV K^+ current amplitude of rEag1-WT channels on any given day of experiment was always normalized as unity. Normalized data from different batches of *Xenopus* oocytes or different days of experiments were later pooled together for comprehensive analyses.

All values were presented as mean ± S.E. The significance of the difference between two means was tested by Student's t test, whereas means from multiple groups were compared by one-way ANOVA. All statistical analyses were performed with the Origin 7.0 software (Microcal Software, Northampton, MA).

Curve fitting and data simulation for the dominant-negative effect of truncation mutants were also performed with Origin 7.0. As have been discussed previously (19), by assuming that WT and nonfunctional mutant subunits are co-expressed with equal efficiency and randomly assemble into a tetramer, binomial theory predicts that the normalized mean current ampli-

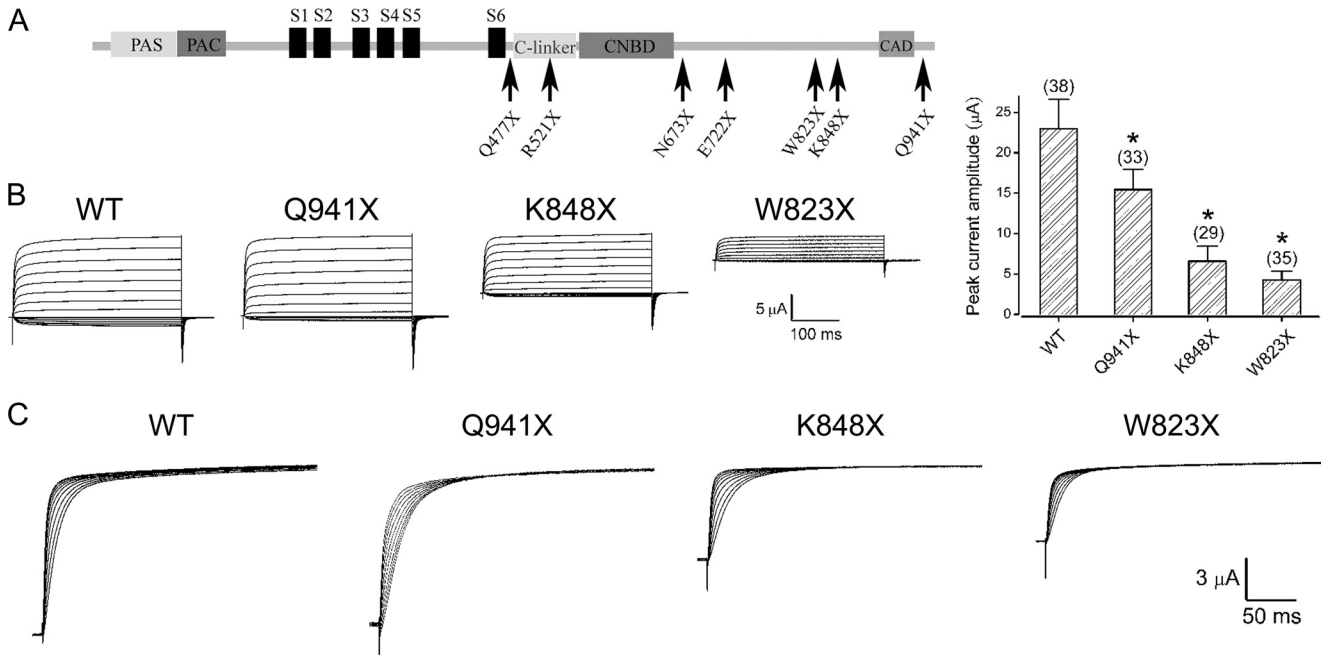

FIGURE 1. **Functional expression of CAD-lacking carboxyl-terminal truncation mutants in *Xenopus* oocytes.** *A,* schematic representation of the location of carboxyl-terminal truncation mutations. The full-length rEag1-WT protein contains 962 amino acids. The carboxyl terminus is characterized by the presence of three distinct regions as follows: C-linker, CNBD, and CAD. Single letter notation is used here to denote the amino acid at the indicated position. A premature stop codon is represented by the letter *X*. *B, left,* representative K^+ currents recorded from oocytes expressing rEag1-WT, Q941X, K848X, or W823X. The bath solution contained 60 mM KCl. The holding potential was −90 mV. The pulse protocol included 370-ms depolarizing test pulses ranging from −70 to +60 mV, with 10-mV increments. *Right,* mean peak current amplitudes at +60 mV measured from oocytes injected with identical concentrations of cRNA for various constructs of rEag1 channels. The recordings were performed 72–96 h post-cRNA injection. The *numbers* in *parentheses* refer to the number of oocytes recorded for each construct. In all figures, *asterisks* denote significant difference from rEag1-WT (*, *t* test: $p < 0.05$). *C,* nonsuperimposable Cole-Moore shift of rEag1-WT and truncation mutants. The bath solution contained 3 mM KCl. The holding potential was −90 mV. The pulse protocol included 300-ms prepulses ranging from −140 to −60 mV, with 10-mV increments, followed by a 300-ms test pulse to +40 mV. Shown here are the current traces in response to the last 10 ms of prepulses and the initial 290 ms of test pulses.

tude (I_{Norm}) can be described as a function of the fraction of mutant subunit (F_{mut}, *e.g.* for 1:1 co-expression, $F_{mut} = 0.5$). If one mutant subunit was sufficient to completely inhibit the function of a tetrameric channel, the predicted function is $I_{Norm} = (1 - F_{mut})^4$ (see Fig. 3*E*, *dashed line A*). One important premise for this function is that WT and mutant subunits oligomerize with equal efficiency and that the suppression effect of the mutant is complete (*i.e.* in an all-or-none manner). If the mutant subunit does not exert any suppression effect against co-assembled WT subunits, the predicted function is $I_{Norm} = 1 - (F_{mut})^4$ (see Fig. 3*E*, *dotted line B*). Consistent with the observation by Flagg *et al.* (19), our data were best fit by an intermediate model, $I_{Norm} = (1 - \alpha F_{mut})^4$ (see Fig. 3*E*, *solid line C*), where α is less than unity and accounts for reduced oligomerization efficiency or partial current inhibition by a single mutant subunit.

Cell Culture and DNA Transfection—Human embryonic kidney (HEK) 293T cells were grown in Dulbecco's modified Eagle's medium (DMEM) supplemented with 2 mM glutamine, 10% heat-inactivated fetal bovine serum (Hyclone, Logan, UT), 100 units/ml penicillin, and 50 μg/ml streptomycin. Cells were maintained at 37 °C in a 95% air and 5% CO_2 humidified incubator and passaged about every 4 days. Transient transfection was performed by using the Lipofectamine 2000 (LF2000) reagent (Invitrogen). Briefly, cells were plated onto 6-well plates (for biochemical experiments) or poly-D-lysine-coated coverslips in 24-well plates (for confocal imaging or electrophysiological recording) 24 h before transfection. Various expression constructs were incubated with LF2000 reagent for 20 min at room temperature, and DNA-Lipofectamine diluted in Opti-MEM (Invitrogen) was added to culture wells containing the plated cells (1 μg of total cDNA/12-mm coverslip). After a 4-h incubation at 37 °C under 5% CO_2, the culture medium was changed, and the culture cells were maintained in a 37 °C incubator for 24–48 h before being used for confocal imaging and electrophysiological or biochemical experiments.

Patch Clamp Recording in HEK293T Cells—Conventional whole-cell patch clamp technique was used to record rEag1 K^+ currents in HEK293T cells. Cells co-transfected with the cDNA for rEag1 and pEGFP (molar ratio 3:1) were identified with a Nikon DIAPHOT-TMD inverted fluorescence microscope (Nikon Corp., Tokyo, Japan). Patch electrodes with a resistance of 2–4 megohms were pulled on a Narishige PP-830 electrode puller (Narishige, Tokyo, Japan) and were filled with a solution containing (in mM) 140 KCl, 1 $MgCl_2$, 10 EGTA, 10 HEPES, pH 7.2. External recording solution consisted of (in mM) 140 NaCl, 5 KCl, 1 $CaCl_2$, and 10 HEPES, pH 7.2. Data were acquired with an Axopatch 200A amplifier (Molecular Devices) and digitized with Digidata 1322A system and pCLAMP 9.0 software. Cell capacitance and series resistance were measured using built-in analytical functions of the pCLAMP 9.0 software and compensated electronically with the Axopatch 200A amplifier. Series resistance was typically 70–80% compensated (with 7–8-μs lag values). The holding potential was set at −90 mV, and passive membrane properties were compensated using the −P/4 leak subtraction method provided by the pCLAMP 9.0 soft-

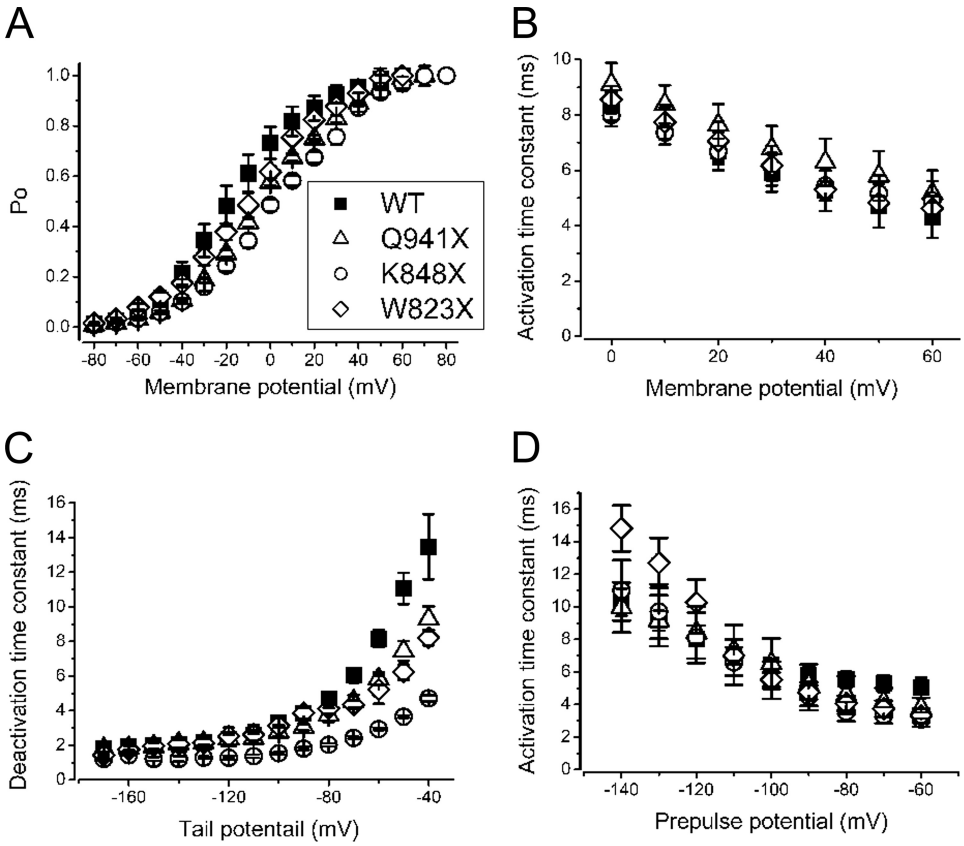

FIGURE 2. **Biophysical properties of the functional truncation mutants Q941X, K848X, and W823X.** *A,* steady-state activation curves of rEag1-WT and truncation mutants. The fraction of open channels (P_o) was plotted against the corresponding test potential (*V*). Data points (n = 8–19) were fit with a Boltzmann equation (*solid curves*). *B,* activation kinetics of rEag1-WT and truncation mutants. Activation time constants (n = 10–18) at indicated potentials were obtained from single exponential fits to the late rising phase of rEag1 currents. *C,* deactivation kinetics of rEag1-WT and truncation mutants. Tail currents were recorded by stepping from +40 mV to potentials ranging from −40 to −170 mV. Deactivation time constants (n = 6–15) were derived from single exponential fits and plotted *versus* tail potential. *D,* nonsuperimposable Cole-Moore shift of rEag1-WT and truncation mutants. Activation time constants at +40 mV (n = 6–16) obtained from single exponential fits to the late rising phase of rEag1 currents are plotted *versus* prepulse potentials.

ware. Data were sampled at 10 kHz and filtered at 1 kHz. Peak K^+ current amplitudes were determined with built-in analytical functions of the pCLAMP 9.0 software. Cells with large currents in which voltage clamp errors might appear were excluded from data analyses. All recordings were performed at room temperature (20–22 °C).

Immunofluorescence—Transfected HEK293T cells were rinsed in PBS and then fixed with 4% paraformaldehyde in PBS ((in mM) 136 NaCl, 2.5 KCl, 1.5 KH_2PO_4, 6.5 Na_2HPO_4, pH 7.4) at 4 °C for 20 min. Cells were washed three times with PBS and then blocked for 30 min in PBS containing 0.1% (v/v) Triton X-100 and 5% normal goat serum. Cells were then incubated overnight at 4 °C in the mouse anti-Myc antibody (clone 9E10) diluted in blocking buffer. After three washes with PBS, the coverslips were incubated with goat anti-mouse antibodies conjugated to Alexa488 (Invitrogen) for 1 h at room temperature. Nuclei were labeled with DAPI. Finally, the coverslips were rinsed once in blocking buffer, twice in PBS, and twice in 0.1 M carbonate buffer, pH 9.2, before they were mounted on glass slides in a mounting medium (4% *n*-propyl gallate, 90% glycerol, 0.1 M carbonate, pH 9.2). The fluorescence images of the fixed cultures were viewed and acquired with a Leica TCS SP2 laser-scanning confocal microscope (Leica, Mannheim, Germany).

Co-immunoprecipitation and Western Blotting—Transfected HEK293T cells were solubilized in ice-cold IP buffer ((in mM) 100 NaCl, 4 KCl, 2.5 EDTA, 20 $NaHCO_3$, 20 Tris-HCl, pH 7.5, 1 phenylmethylsulfonyl fluoride, 1% Triton X-100) containing protease inhibitor mixture (Roche Applied Science). Insolubilized materials were removed by centrifugation. Solubilized lysates were incubated for 16 h at 4 °C with protein G-Sepharose (GE Healthcare) previously coated with anti-Myc antibodies (clone 9E10). Beads were washed three times in IP buffer and twice with IP buffer with Triton X-100. The immune complexes were eluted from the beads by boiling for 5 min in Laemmli sample buffer. Protein in the cell lysates or immunoprecipitated samples were separated on 7.5% SDS-polyacrylamide gels, transferred to nitrocellulose membranes, and detected using mouse anti-Myc (clone 9E10), rabbit anti-GFP antibodies (1:1000; Abcam, San Francisco), mouse anti-β-actin (1:10,000; Sigma), or rabbit anti-rEag1 (1:10,000; Alomone Labs, Jerusalem, Israel) antibodies. Blots were then exposed to horseradish-peroxidase conjugated anti-mouse or anti-rabbit IgG antibodies (1:5000; Thermo Scientific, Rockford, IL) and revealed by an enhanced chemiluminescence detection system (Western Lightning detection kit, PerkinElmer Life Sciences).

Biotinylation of Cell Surface Proteins—Transfected HEK293T cells were washed extensively with PBS supplemented with 0.5 mM $CaCl_2$, 2 mM $MgCl_2$ (CM/PBS), followed by incubation in 1 mg/ml

sulfo-NHS-LC-biotin (Thermo Scientific) in CM/PBS at 4 °C for 30 min with gentle rocking. Biotinylation was terminated by removing the biotin reagents and rinsing three times each with CM/PBS and TBS. Cells were solubilized in RIPA buffer ((in mM) 20 Tris-HCl, 150 NaCl, 1% Triton X-100, 0.5% sodium deoxycholate, 0.1% SDS, 1 EDTA, 1 phenylmethylsulfonyl fluoride, pH 7.4) supplemented with protease inhibitor mixture. Insolubilized material was removed by centrifugation. Solubilized cell lysates were incubated for 16 h at 4 °C with streptavidin-agarose beads (Thermo Scientific). Beads were washed three times in lysis buffer and twice with TBS. The biotin-streptavidin complexes were eluted from the beads by boiling for 5 min in Laemmli sample buffer and were subjected to SDS-PAGE and immunoblotting.

Glycosidase Treatment—The detergent-soluble fraction of transfected HEK293T cells was analyzed for *N*-glycosidase F (PNGase F) and endoglycosidase H (Endo H) (New England Biolabs, Ipswich, MA) by following the manufacturer's protocol. In brief, cell extracts were prepared in ice-cold RIPA buffer by rocking for 30 min at 4 °C and cleared by centrifugation (16,000 × *g*, 10 min, 4 °C). Protein concentrations were determined by the BCA method (Thermo Scientific). Equal amounts of proteins (20 μg) were treated with 1000 units of PNGase F or Endo H for 1 h at 37 °C, separated by SDS-PAGE, transferred to nitrocellulose membranes, and subjected to Western blotting analysis.

RESULTS

CAD-lacking rEag1 Subunits Can Form Functional K^+ Channels—As illustrated in Fig. 1*A*, the carboxyl terminus of rEag1 channel encloses three distinct domains as follows: C-linker (~90 amino acids), CNBD (~120 amino acids), and CAD (41 amino acids) (11, 20). Although C-linker and CNBD constitute approximately the proximal half of rEag1 carboxyl terminus, CAD is located toward the end of the distal half. To address whether CAD is the principal assembly domain for Eag channels, we began with constructing a series of rEag1 truncation mutations in the carboxyl terminus. Q941X was the only mutant with an intact CAD. K848X, W823X, E722X, and N673X contained C-linker and CNBD but no CAD. Only a partial segment of C-linker and thus no CNBD was present in R521X, whereas there was virtually no carboxyl terminus in Q477X.

We then evaluated the functional expression of these truncation mutants by performing two-electrode voltage clamp recordings in *Xenopus* oocytes. As expected, Q941X was able to form functional K^+ channels that were virtually indistinguishable from that for WT (Fig. 1*B*). Despite applying the highest concentrations of cRNA for injection and up to 96 h of post-injection incubation time, the four shorter mutants (E722X, N673X, R521X, and Q477X) appeared nonfunctional in *Xenopus* oocytes (data not shown). Surprisingly, the other two CAD-lacking truncation mutants, K848X and W823X, did produce functional K^+ currents (Fig. 1*B*). Although the two mutants yielded smaller maximal current amplitudes (Fig. 1*B*), the time course of their functional expression in *Xenopus* oocytes was identical to that for WT, all reaching a steady level at 48–72 h post-cRNA injection. Moreover, both K848X and W823X channels displayed a significant delay in activation kinetics in response to hyperpolarizing prepulses (Fig. 1*C*), a characteristic Eag feature also known as the nonsuperimposable Cole-Moore shift (21–23). In general, the biophysical phenotypes of K848X and W823X were quite similar to those of rEag1-WT (Fig. 2), although both mutants displayed a right-shifted steady-state activation curve, as well as a notable acceleration of the deactivation kinetics (Tables 1 and 2).

CAD-lacking Nonfunctional Truncation Mutants Display Dominant-negative Effects on rEag1 K^+ Channels—As mentioned above, four of the carboxyl-terminal truncation mutants (E722X, N673X, R521X, and Q477X) failed to generate functional K^+ channels in *Xenopus* oocytes. If CAD is indeed indispensable for the assembly of rEag1 subunits, then these nonfunctional mutants would not be expected to co-assemble with their WT counterpart. To test this hypothesis, we co-expressed each truncation mutant individually with rEag1-WT subunit in 1:1 molar ratio to determine whether the expression of rEag1 K^+ currents would be suppressed in *Xenopus* oocytes. The assumption for this experiment is that WT and mutant subunits express equally and assemble randomly. Furthermore, based on the assumption that two mutant subunits suffice to block a hetero-tetrameric channel, binomial distribution predicts that in 1:1 molar ratio of WT-mutant co-expression, a significant dominant-negative effect should result in a reduction of current amplitude by at least 37% (24). Voltage clamp recordings were performed 48–72 h post-cRNA injection, corresponding to the peak expression time point for WT. As

TABLE 1
Comparison of the steady-state voltage-dependent activation property

	$V_{0.5}$	Slope factor
	mV	*mV*
WT	−15.4 ± 0.9	19.7 ± 0.8
Q941X	−3.1 ± 0.7[a]	18.7 ± 0.6
K848X	+3.1 ± 0.8[a]	20.0 ± 0.7
W823X	−10.2 ± 0.5[a]	19.3 ± 0.5

[a] Data are significantly different from WT; *t*-test, $p < 0.05$.

TABLE 2
Comparison of the deactivation kinetics
Deactivation time constant (τ) was determined by one-exponential fit to the tail current recorded at the indicated tail potential (V_{Tail}) (n = 16–24).

	Deactivation τ						
V_{Tail}	-40	−60	−80	−100	−120	−140	−160
mV				*ms*			
WT	13.5 ± 1.9	8.2 ± 0.5	4.7 ± 0.3	3.3 ± 0.3	2.3 ± 0.3	2.1 ± 0.2	1.9 ± 0.2
Q941X	9.3 ± 0.7[a]	5.8 ± 0.4[a]	3.7 ± 0.4	2.8 ± 0.2	2.4 ± 0.4	2.1 ± 0.4	1.8 ± 0.2
K848X	4.7 ± 0.2[a]	2.9 ± 0.1[a]	2.9 ± 0.1[a]	1.5 ± 0.1[a]	1.3 ± 0.1[a]	1.2 ± 0.2[a]	1.2 ± 0.2[a]
W823X	8.2 ± 0.4[a]	5.2 ± 0.8[a]	4.1 ± 0.3	3.1 ± 0.1	2.5 ± 0.5	2.1 ± 0.2	1.8 ± 0.2

[a] Data are significantly different from WT; *t*-test, $p < 0.05$.

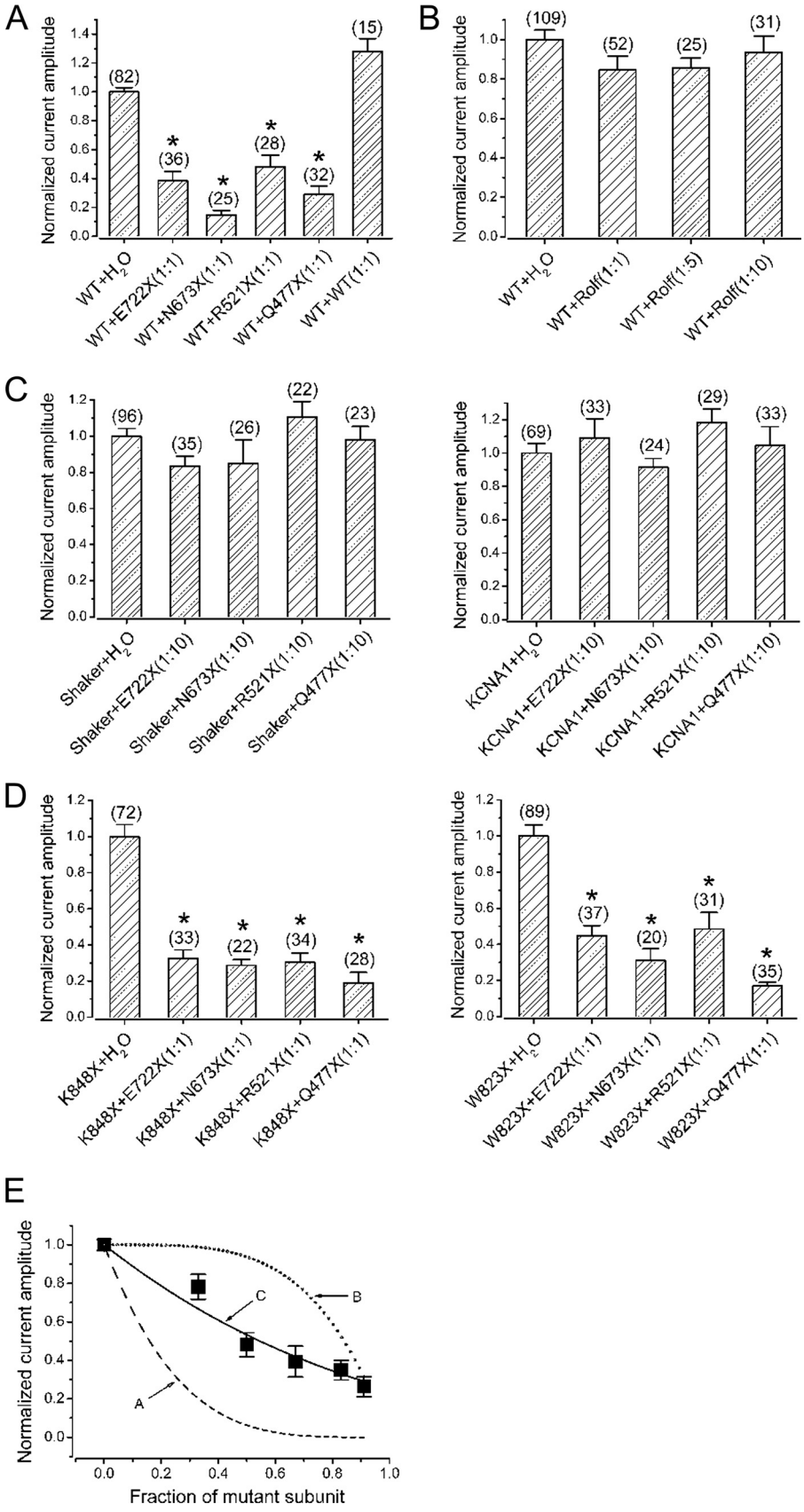
A
Normalized current amplitude
(82)
(36)
(25)
(28)
(32)
(15)
WT+H2O
WT+E722X(1:1)
WT+N673X(1:1)
WT+R521X(1:1)
WT+Q477X(1:1)
WT+WT(1:1)
B
(109)
(52)
(25)
(31)
WT+H2O
WT+Rolf(1:1)
WT+Rolf(1:5)
WT+Rolf(1:10)
C
(96)
(35)
(26)
(22)
(23)
Shaker+H2O
Shaker+E722X(1:10)
Shaker+N673X(1:10)
Shaker+R521X(1:10)
Shaker+Q477X(1:10)
(69)
(33)
(24)
(29)
(33)
KCNA1+H2O
KCNA1+E722X(1:10)
KCNA1+N673X(1:10)
KCNA1+R521X(1:10)
KCNA1+Q477X(1:10)
D
(72)
(33)
(22)
(34)
(28)
K848X+H2O
K848X+E722X(1:1)
K848X+N673X(1:1)
K848X+R521X(1:1)
K848X+Q477X(1:1)
(89)
(37)
(20)
(31)
(35)
W823X+H2O
W823X+E722X(1:1)
W823X+N673X(1:1)
W823X+R521X(1:1)
W823X+Q477X(1:1)
E
Normalized current amplitude
A
B
C
Fraction of mutant subunit

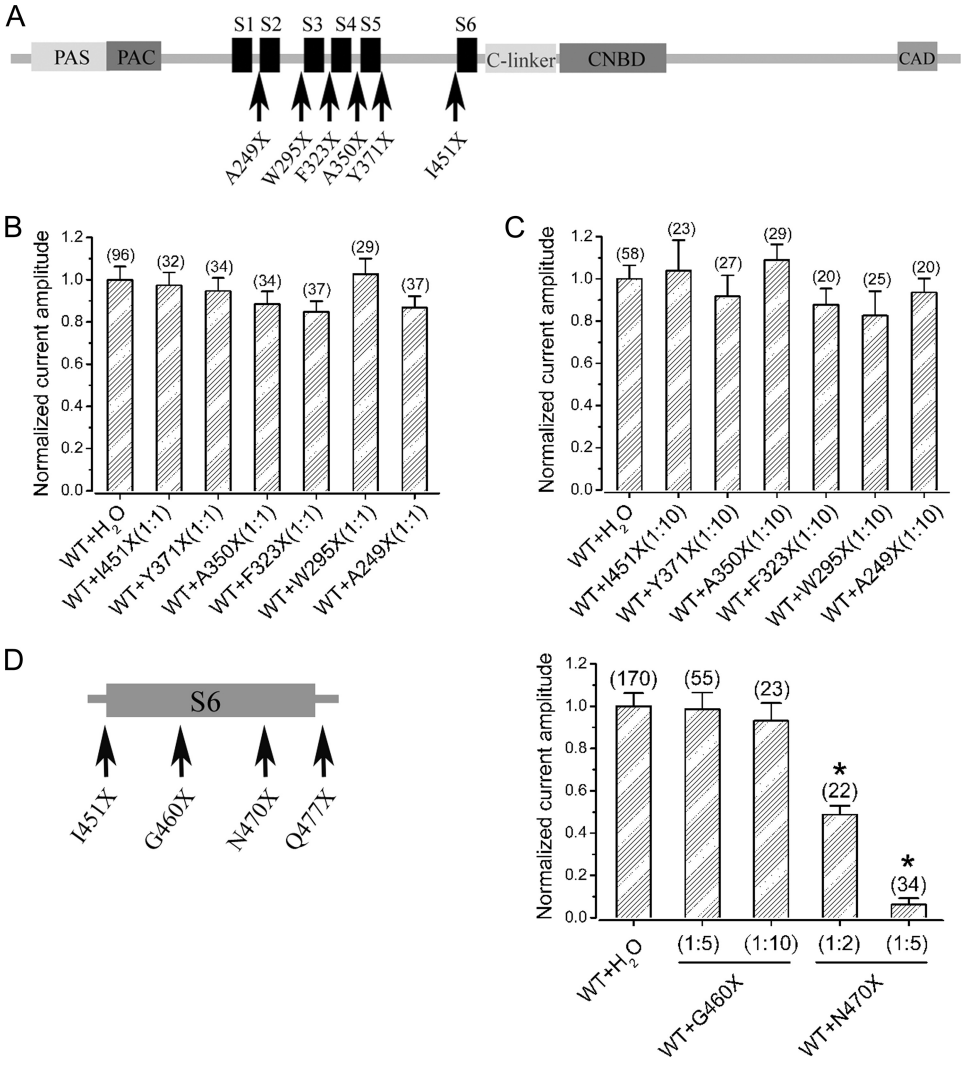

FIGURE 4. **All but S6 transmembrane domain truncation mutants fail to display dominant-negative effects in *Xenopus* oocytes.** *A,* schematic representation of the location of transmembrane S1-Pore domain truncation mutations. None of these six truncation mutants generated functional K^+ channels in oocytes (data not shown). Equal molar (*B*) or 10-fold excess (*C*) co-expression with the transmembrane domain truncation mutants did not significantly affect the mean K^+ current amplitudes of rEag1-WT channels (one-way ANOVA: $p > 0.05$). *D, top,* schematic representation of the location of the two S6 domain truncation mutations, both of which failed to generate functional K^+ channels in oocytes (data not shown). *Bottom,* N470X, but not G460X, displayed significant dominant-negative effect.

depicted in Fig. 3*A*, in the presence of the CAD-lacking mutants, rEag1 current amplitudes at +60 mV dramatically decreased by about 50–85%. Enhancing the co-expression ratio of the truncation mutants to 1:5 or 1:10 led to further reduction of the WT current amplitude (Fig. 3*E*). Moreover, co-expression with CAD-lacking mutants failed to significantly affect the kinetic property, as well as the steady-state voltage activation, of rEag1-WT (data not shown). Together, these data suggest that all four truncation mutants exerted significant dominant-negative effects on rEag1-WT subunits.

To rule out the possibility that the observed current reduction may arise from nonspecific suppression of protein expression imposed by the truncation mutants, we replaced the truncation mutants with rat olfactory channel (Rolf; a cyclic nucleotide-gated channel α-subunit), a protein that was not known to interact with rEag1 subunit, for co-expression exper-

FIGURE 3. **Dominant-negative effects of nonfunctional carboxyl-terminal truncation mutants in *Xenopus* oocytes.** *A,* normalized mean K^+ current amplitudes of rEag1-WT channels in the absence or presence of nonfunctional carboxyl-terminal mutants. The pulse protocol was identical to that shown for Fig. 1*B*. *B,* normalized mean K^+ current amplitudes of rEag1-WT channels in the presence of different molar ratios of Rolf. The mean amplitudes of K^+ currents through rEag1-WT channels in the absence (WT + H_2O) or presence of Rolf (molar ratios 1:1, 1:5, and 1:10) were not significantly different (one-way ANOVA: $p > 0.05$). *C,* normalized mean K^+ current amplitudes of Shaker (*left*) or KCNA1 (*right*) channels in the absence or presence of rEag1 nonfunctional carboxyl-terminal mutants. 10-Fold excess co-expression with the rEag1 truncation mutants failed to significantly alter the K^+ current amplitudes of either Shaker or KCNA1 channels (one-way ANOVA: $p > 0.05$). *D,* normalized mean K^+ current amplitudes of rEag1-K848X (*left*) or -W823X (*right*) channels in the absence or presence of nonfunctional carboxyl-terminal mutants. *E,* co-expression of WT and E722X in different molar ratios. rEag1-WT and E722X were co-expressed in oocytes in the molar ratios of 1:0, 1:0.5, 1:1, 1:2, 1:5, and 1:10, with a fixed mount of WT cRNA in all conditions. The *dashed line* A refers to the predicted function $I_{Norm} = (1 - F_{mut})^4$, where I_{Norm} and F_{mut} stand for normalized mean current amplitude and fraction of mutant subunit, respectively. The *dotted line B* corresponds to the predicted function $I_{Norm} = 1 - (F_{mut})^4$. The *solid line* (*C*) represents a best fit ($R^2 = 0.96$) to the dominant-negative effect of E722X by the function $I_{Norm} = (1 - \alpha F_{mut})^4$, with $\alpha = 0.3$. See under "Experimental Procedures" for more detail. Data were collected from 12 to 25 oocytes for each co-expression ratio.

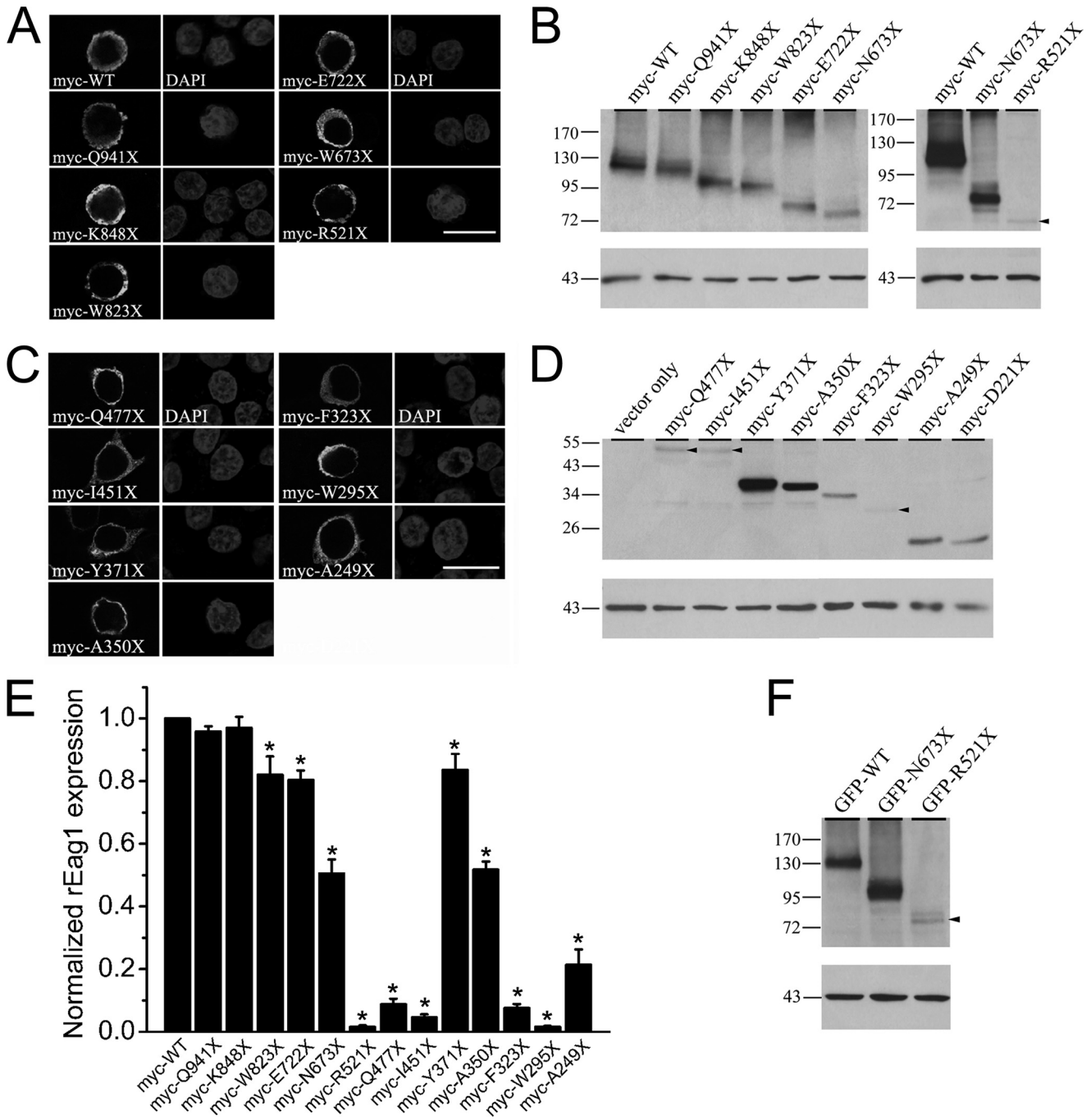

FIGURE 5. **Protein expression of truncation mutants in HEK293T cells.** *A,* immunofluorescence staining patterns of HEK293T cells expressing Myc-tagged rEag1 carboxyl-terminal mutants. Fixed cells were stained with anti-Myc antibody (*left*) as well as the nuclear counterstain DAPI (*right*), followed by imaging with confocal microscopy. *Scale bar,* 20 μm. *B,* Western blotting analyses of Myc-tagged rEag1 carboxyl-terminal mutants (*left*). The protein signal for R521X (*arrowhead*) was resolved upon prolonging detection time of immunoblot (*right*). The positions of molecular mass markers (in kilodaltons) are indicated to the *left* of the blots. The apparent molecular mass of rEag1-WT is about 110–120 kDa. Corresponding β-actin expression levels for each lane are displayed in the *lower panels*. *C,* confocal images of Myc-tagged rEag1 transmembrane domain mutants. *Scale bar,* 20 μm. *D,* Western blotting analyses of vector control, as well as Myc-tagged rEag1 transmembrane domain mutants. The protein bands corresponding to Q477X, I451X, and W295X are highlighted with *arrowheads*. *E,* quantification of rEag1 protein expression level. Protein density was standardized as the ratio of myc-rEag1 signal to cognate β-actin signal. Values from various rEag1 truncation mutants were then normalized with respect to those for WT. Densitometric scans of immunoblots were obtained from five independent experiments. *F,* Western blotting analyses of GFP-tagged WT, N673X, and R521X.

iments with rEag1-WT. As illustrated in Fig. 3*B*, co-expressing with Rolf to a molar ratio of 1:10 failed to significantly alter rEag1 current amplitudes at +60 mV. Moreover, when we employed two members of Kv1 channel family, Shaker and KCNA1 channels, to replace rEag1-WT for co-expression experiments, no significant dominant-negative effects were observed (Fig. 3*C*), indicating that the truncation mutants did not exert promiscuous suppression effects on K^+ channels of a different subfamily.

To further evaluate the role of CAD in rEag1 subunit interactions, we asked whether the CAD-lacking nonfunctional truncation mutants could display dominant-negative effects on

the two CAD-lacking functional channels K848X and W823X. Fig. 3*D* demonstrated that indeed the current expression of both K848X and W823X was significantly suppressed in the presence of their nonfunctional counterparts. These data therefore strongly suggest that CAD may be dispensable for the interaction of rEag1 subunits.

As shown in Fig. 1*A*, there was virtually no carboxyl terminus in the truncation mutant Q477X, which, however, could still exert a strong dominant-negative effect. This observation raised an interesting possibility that the transmembrane domains may also contribute to the assembly of rEag1 subunits, as have been previously demonstrated for Kv1.3 channels (25). To address this hypothesis, we made another series of six truncations over the transmembrane domain (Fig. 4*A*). The shortest mutant A249X contained the amino terminus and S1 segment only, whereas the longest construct I451X terminated right before the beginning of the S6 segment. As demonstrated in Fig. 4, *B* and *C*, in both 1:1 and 1:10 co-expression molar ratios, none of these seven mutants exhibited significant current suppression effects on rEag1-WT. A similar result was also observed when we increased the post-injection incubation time up to 96 h (data not shown).

Because Ile^{451} and Gln^{477} are located at the beginning and the end of the S6 segment, respectively, the preceding results imply that the critical transmembrane domain for generating the dominant-negative effects may predominantly reside in the S6 segment. To further test this hypothesis, we generated two additional truncation mutants over the S6 segment, G460X and N470X. Gly^{460} is located at approximately the middle of the S6 segment, whereas Asn^{470} is about halfway between Gly^{460} and Gln^{477}. As depicted in Fig. 4*D*, only N470X, but not G460X, displayed significant suppression effect against rEag1-WT. Together, our data suggest that the distal half of the S6 segment may be essential for the dominant-negative effect of CAD-lacking truncation mutants.

CAD Is Dispensable for the Interaction of rEag1 Subunits—The *Xenopus* oocyte is a very efficient expression system in that a high copy number of RNA molecules can be achieved via *in vitro* transcription and that the quality control system for protein folding and trafficking is less stringent in this type of amphibian cell (26). Therefore, to ensure the foregoing results on CAD-lacking truncation mutants were not expression system-dependent phenomena, we then switched to the mammalian expression system HEK293T cells for further analyses. We first employed Myc-tagged constructs for protein expression studies. Fig. 5*A* illustrates the immunofluorescence images of the longer truncation mutants that were over 500 amino acids in length, *i.e.* from R521X through Q941X. All six mutant constructs were able to produce proteins in HEK293T cells, although the expression efficiency was significantly lower for the shortest mutant R521X. This observation was further supported by Western blotting analyses with the anti-Myc antibody (Fig. 5*B*). The expression efficiency of myc-R521X, however, was so low that we could barely detect its signal by Western blotting. Alternatively, this may imply the Myc epitope in myc-R521X was not quite accessible for immunoblotting experiments. The protein signal of R521X was improved when we switched to the GFP epitope but was still

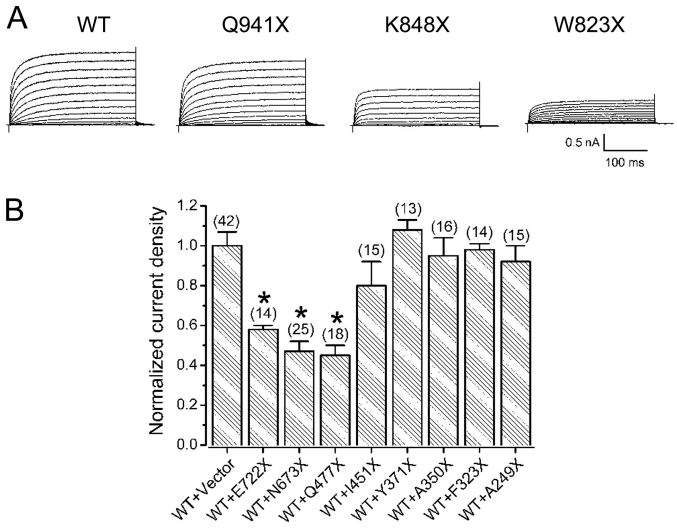

FIGURE 6. **Functional expression of CAD-lacking rEag1 mutants in HEK293T cells.** *A,* representative K^+ currents recorded from HEK293T cells expressing rEag1-WT Q941X, K848X, or W823X. The holding potential was −90 mV. The pulse protocol included 300-ms depolarizing test pulses ranging from −90 to +50 mV, with 10-mV increments. All the other truncation mutants failed to produce functional K^+ channels in HEK293T cells (data not shown). *B,* normalized mean K^+ current density (at +40 mV) of rEag1-WT channels in the absence or presence of nonfunctional truncation mutants. HEK293T cells were co-transfected in equal-molar ratios with cDNA for rEag1-WT and vector (WT + vector) or the indicated truncation mutant.

relatively low when compared with other constructs (Fig. 5*F*). Fig. 5, *C* and *D,* depict the immunofluorescence and Western blotting results, respectively, of the remaining Myc-tagged truncation mutants. All seven shorter mutant constructs generated detectable immunofluorescence signals in HEK293T cells, but the protein expression efficiency was considerably lower for myc-W295X. Fig. 5*E* illustrates the quantitative summary of the relative protein expression level. Together, these data indicate that the mutants W295X and R521X displayed significantly defective expression efficiency and were thus unsuitable for further analyses in HEK293T cells.

We next examined the functional properties of the truncation mutants by performing whole-cell patch clamp recordings in the mammalian expression system. Consistent with the findings from oocytes, only Q941X and the two CAD-lacking mutants W823X and W848X produced functional K^+ channels in HEK293T cells (Fig. 6*A*). Similarly, when we co-expressed in HEK293T cells the nonfunctional truncation mutants with their WT counterpart, only the mutants Q477X, N673X, and E722X produced significant dominant-negative effects on rEag1-WT channels (Fig. 6*B*). The dominant-negative effect of Q477X was impressive because its protein expression level was significantly lower than those of shorter mutants such as A350X and Y371X (Fig. 5, *D* and *E*), implying again that Q477X may contain a non-CAD structural domain that can efficiently interact with rEag1 subunits.

So far, in both *Xenopus* oocytes and HEK293T cells, we have presented functional evidence suggesting that CAD-lacking truncation mutants may possess significant subunit-interacting capacities. To directly verify the presence of this subunit interaction potential, we also performed a series of co-immunoprecipitation experiments. We began with the carboxyl-terminal truncation mutants N673X, E722X, W823X, K848X, and

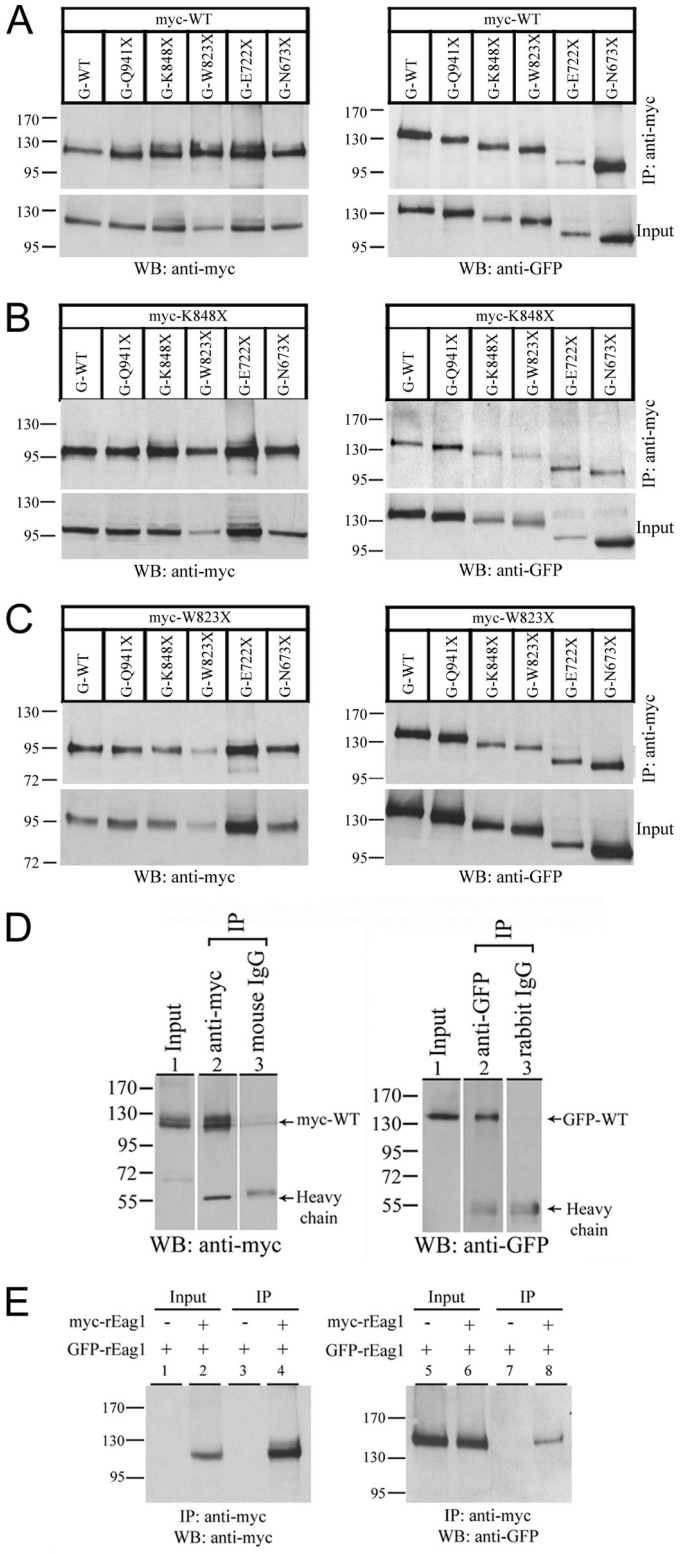

FIGURE 7. **Interaction of CAD-lacking rEag1 subunits in HEK293T cells.** Myc-tagged rEag1-WT (*A*), K848X (*B*), or W823X (*C*) was co-transfected with the indicated GFP-tagged rEag1 subunit construct into HEK293T cells. Cell lysates were immunoprecipitated (*IP*) with anti-Myc antibody (*upper panels*). rEag1 proteins were detected by immunoblotting (*WB*) with anti-Myc (*left*) or anti-GFP (*right*) antibodies. Corresponding expression levels of Myc- or GFP-tagged constructs in the lysates (*Input*) are shown in the *lower panels*. In all cases hereafter, input represents 5% of the total protein used for immunoprecipitation. *D,* specificity of the immunoprecipitation procedure was verified by the absence of the myc-rEag1 protein band when mouse anti-Myc IgG was replaced by a nonspecific mouse IgG. *E,* specificity of the co-immunoprecipitation experiment was confirmed by replacing Myc-tagged rEag1 (+) with Myc vector (−) for co-transfection with GFP-rEag1. Immunoprecipitation was carried out by using anti-Myc antibody, whereas immunoblotting was performed by using anti-Myc (*left*) or anti-GFP (*right*) antibody. Vector replacement led to the absence of the immunoreactive band for either Myc- or GFP-tagged rEag1 subunit.

Q941X. By epitope tagging WT and mutants with Myc and GFP, respectively, we demonstrated that WT and the CAD-lacking subunits indeed co-existed in a protein complex (Fig. 7*A*). Moreover, subunit interaction between CAD-lacking subunits was revealed by the finding that both Myc-tagged K848X and W823X mutants were co-immunoprecipitated with GFP-tagged truncation mutants (Fig. 7, *B* and *C*). The specificity of our anti-Myc and -GFP antibodies for both immunoprecipitation and immunoblotting was exemplified in Fig. 7, *D* and *E*.

Another critical question that we have yet to address is as follows. Can the subunit interaction patterns shown in Fig. 7 be specific enough to account for the dominant-negative effects of the nonfunctional mutants? To tackle this question, we first focused on the three mutants E722X, Y371X, and A350X, of which only E722X displayed dominant-negative effects on rEag1-WT channels (see Figs. 3 and 6). As depicted in Fig. 8*A*, all three mutants were co-immunoprecipitated with rEag1-WT subunits. The co-immunoprecipitation efficiency of E722X, however, was significantly better, even though the protein expression level of E722X was no higher than that for Y371X (see also Fig. 5*E*). Next, we compared E722X, Q477X, and F323X, of which only F323X failed to exhibit a significant dominant-negative effect. As shown in Fig. 8*B*, both Q477X and F323X were co-immunoprecipitated with rEag1-WT subunits, with F323X yielding a significantly lower efficiency. Therefore, these data suggest that a direct interaction with rEag1-WT subunits *per se* does not necessarily imply the existence of a significant dominant-negative effect. Nevertheless, those mutants showing dominant-negative effects do tend to display higher association efficiency with their WT counterpart.

CAD-lacking Truncation Mutants Demonstrate Defective Membrane Trafficking and Protein Glycosylation—If CAD interaction is not crucial for the assembly of tetrameric organization, what else could be its significance in the biosynthesis of rEag1 channels? We noticed in both *Xenopus* oocytes and HEK293T cells that the maximal current amplitudes of K848X and especially W823X were smaller than that for WT; furthermore, R521X displayed an exceptionally defective protein expression in HEK293T cells. Hence, one potential role of CAD, as well as other regions within the distal carboxyl terminus, may be related to membrane trafficking and/or protein biogenesis. To address this hypothesis, we first compared the surface expression efficiency of rEag1-WT with that of the carboxyl-terminal truncation mutants Q941X, K848X, W823X, E722X, and N673X. Among these five mutants, Q941X was the only one with an intact CAD. As demonstrated by the protein biotinylation results in Fig. 9, *A* and *B*, the surface expression ratio of the four CAD-lacking mutants was lower than that of WT, with the longer mutants (K848X, W823X, and E722X) decreasing by about 15–30%, and the shortest mutant N673X showed a dramatic reduction by about 70%. This deficiency in

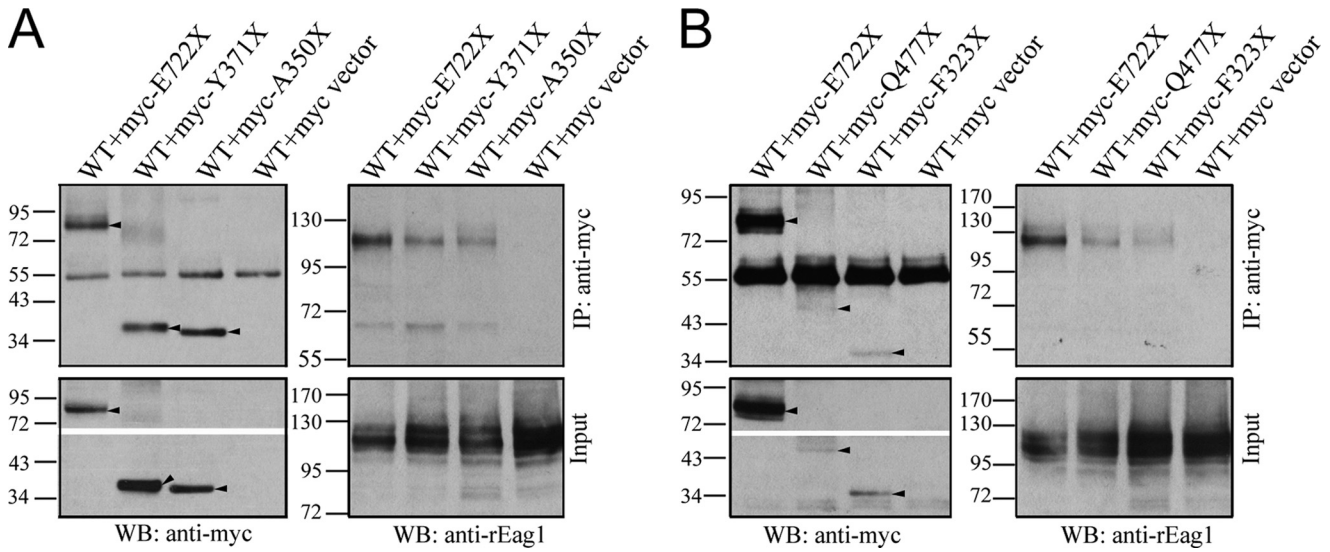

FIGURE 8. **Subunit association efficiency with rEag1-WT, carboxyl-terminal *versus* transmembrane domain truncation mutants.** rEag1-WT subunit was co-immunoprecipitated with Myc-tagged truncation mutants (E722X, Y371X, or A350X (*A*); E722X, Q477X, or F323X (*B*)) or pcDNA3 vector (vector only). Cell lysates were immunoprecipitated (*IP*) with anti-Myc antibody. rEag1-WT and Myc-tagged mutants were detected by immunoblotting (*WB*) with anti-rEag1 (*right*) and anti-Myc (*left*) antibodies, respectively. The epitope sequence for anti-rEag1 antibody (802–817) was absent in these truncation mutants. *Arrowheads* denote the protein band matching the listed truncation mutant in each lane. The 55-kDa bands on *left panels* correspond to the heavy chain of mouse anti-Myc IgG.

membrane trafficking efficiency was unlikely to be attributed to variations in the integrity of plasma membrane during biotinylation experiments, as the cytoplasmic β-actin was not detected in the fraction of proteins retained by streptavidin (Fig. 9*A*, *upper panel*). Interestingly, the membrane trafficking efficiency of WT subunits was comparable in the absence or presence of truncation mutants such as E722X (Fig. 9*C*), suggesting that the dominant-negative effect of the mutants does not seem to be related to reduced surface expression of WT homotetramers.

An important step during the biogenesis of membrane protein is the conversion of its glycosylation pattern from core (high mannose oligosaccharides) into mature (complex) glycans. Human Eag1 channel has been shown to be *N*-glycosylated at two residues in the S5-S6 linker region (27). Immunoblot analysis of HEK293T cells transfected with rEag1-WT subunits revealed two bands with apparent molecular masses of about 110–120 kDa (Fig. 10), similar to the pattern identified in human Eag1 (27). Both protein bands collapsed into a single band with a smaller molecular weight upon pretreatment of the cells with PNGase F (Fig. 10), which is an amidase that removes all *N*-linked oligosaccharides from glycosylated proteins. In contrast, the apparent molecular weight of the lower band, but not the upper band, of rEag1-WT shifted downward in response to pretreatment with Endo H (Fig. 10), which cleaves high mannose oligosaccharides from core-glycosylated immature glycoproteins that have yet to exit from the endoplasmic reticulum during the early stage of biogenesis. These glycosidase digestion results therefore suggest that the upper and lower protein band corresponds to the mature Golgi-processed form and the immature core-glycosylated form, respectively, of rEag1-WT subunits. The CAD-containing mutant Q941X also clearly displayed double bands with glycosidase digestion patterns comparable with those of WT (Fig. 9). For all the other four mutants, however, the immunoblot signal for the upper band was significantly decreased, and only a vague mature glycan form was identified upon Endo H digestion for the two shortest mutants E722X and N673X (Fig. 10), implying that the majority of these CAD-lacking mutant proteins fail to acquire the mature Golgi-processed glycan structure.

DISCUSSION

During the biogenesis of Kv1 channels, intersubunit associations via the tetramerization domain are considered the initial step of tetramerization but may not be required for ensuing steps in channel assembly (28, 29). Conversely, nontetramerization domains may also take place due to promiscuous associations of transmembrane core regions (25, 29, 30). The main question here is thus whether identification of functional CAD-lacking mutants *per se* justifies a re-consideration of the role of CAD in Eag channels.

We think there are three major lines of evidence against the idea that CAD constitutes the primary recognition site for intersubunit associations. First, the time course of the functional expression of K848X and W823X was identical to that for WT, all reaching a steady level at 48–72 h post-cRNA injection and 24–48 h post-cDNA transfection in *Xenopus* oocytes and HEK293T cells, respectively. This observation is in direct contrast with a Shaker T1-lacking mutant that displayed a significantly slower expression time course (29), and it implies that the assembly kinetics of rEag1 subunit tetramerization are comparable in the absence or presence of CAD. Second, the dominant-negative effects of nonfunctional CAD-lacking mutants seem to be Eag-specific, as the mutants failed to exert any significant suppression on Kv1 channels. By contrast, T1-lacking Kv1.3 subunits were shown to display promiscuous interaction with Kv2.1 channels (25). Furthermore, both our functional and biochemical data support the idea that nonfunctional CAD-lacking mutants can efficiently interact with K848X/W823X, suggesting that very proficient rEag1 subunit associations may still occur in the absence of CAD. Third,

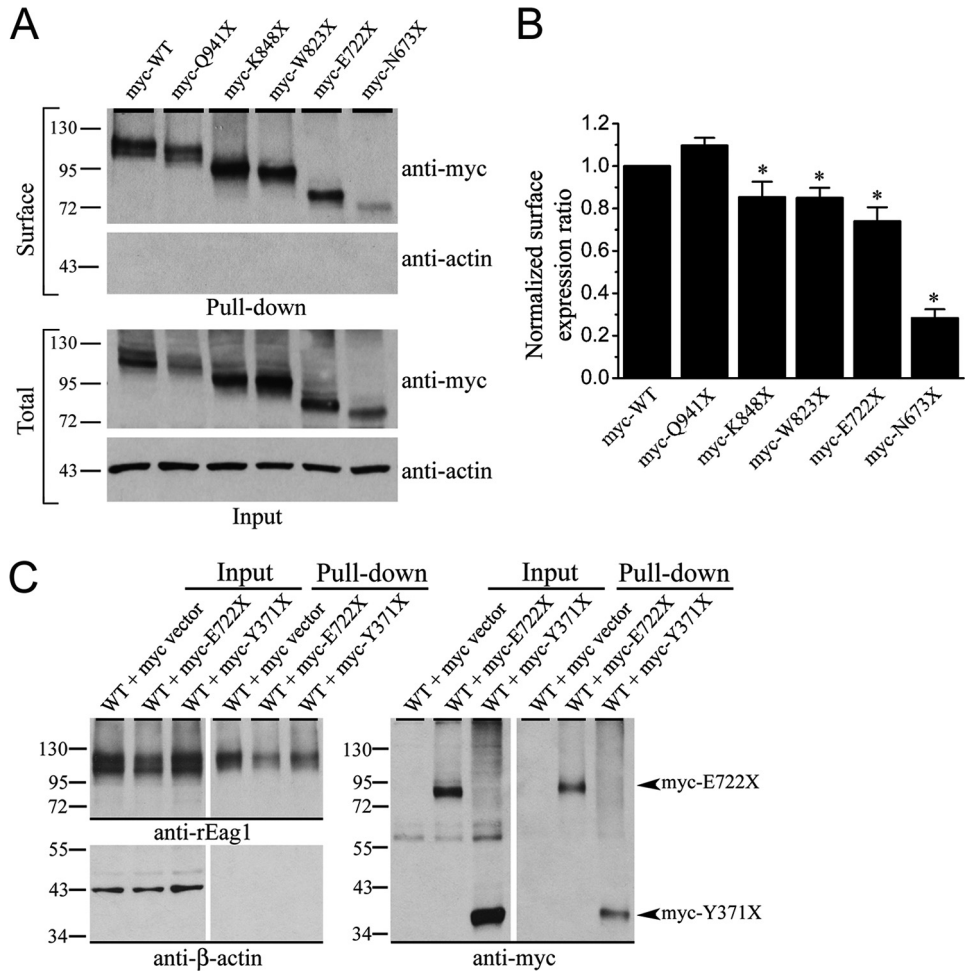

FIGURE 9. **Surface expression efficiency of carboxyl-terminal truncation mutants.** *A,* surface biotinylation experiments on HEK293T cells expressing Myc-tagged rEag1-WT or truncation mutants. Intact cells were biotinylated on ice and thereafter solubilized. *Surface,* cell lysates were pulled down with streptavidin-agarose beads (*Pull-down*) and immunoblotted with anti-Myc or anti-β-actin antibody. *Total,* cell lysates were directly employed for immunoblotting analyses. The specificity of the biotinylation procedure was verified by the absence of the immunoreactive band for β-actin in the pulldown fraction. *B,* quantification of surface expression efficiency. For each rEag1 construct, the total protein density was standardized as the ratio of input signal to cognate β-actin signal. The efficiency of surface presentation was then expressed as surface protein density divided by corresponding standardized total protein density. The mean surface expression ratio of each truncation mutant was subsequently normalized with respect to that of WT. Densitometric scans of immunoblots were obtained from three to five independent experiments. *C,* surface expression of WT and mutant proteins under co-expression condition.

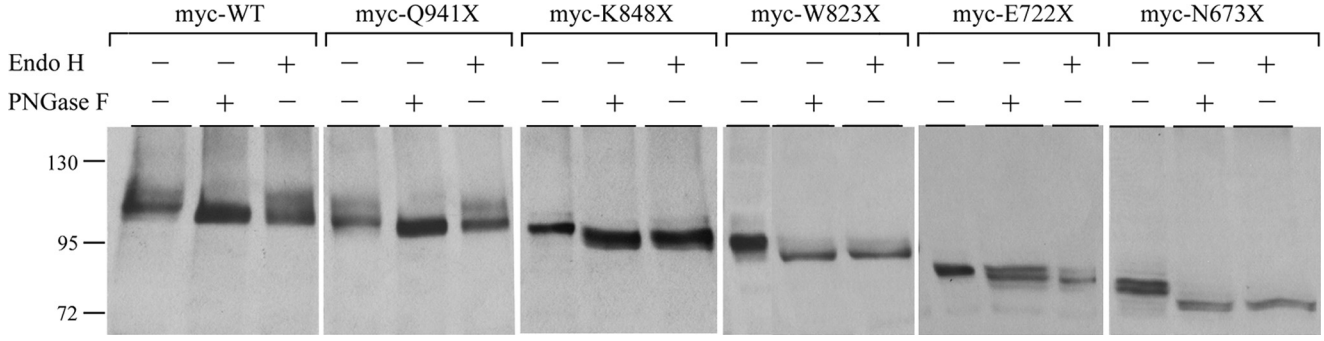

FIGURE 10. **Glycosylation pattern of carboxyl-terminal truncation mutants.** Lysates from HEK293T cells expressing the indicated Myc-tagged rEag1 construct were either untreated (*1st lane*) or treated with PNGase F (*2nd lane*) or Endo H (*3rd lane*). The four shorter truncation mutants (K848X, W823X, E722X, and N673X) showed a significantly less complex glycan form that was predominantly Endo H-sensitive.

although a coiled-coil conformation (TCC) has been demonstrated for a CAD-analogous carboxyl-terminal region in Erg channels (12), the precise significance of TCC remains controversial. For example, the removal of the TCC region via a truncation of over 200 carboxyl-terminal residues failed to prevent tetramer formation in Erg channels (16).

If not CAD, then where else may serve as the primary assembly domain for rEag1 subunit interaction? We have shown that at least in *Xenopus* oocytes, N470X, which includes about three-quarters of the S6 segment, constitutes the shortest truncation mutant that displays significant dominant-negative effect on WT current. In addition, the S6 segment-containing

Q477X also exhibits a significant suppression effect as well as efficient subunit association. These data suggest that the distal half of the S6 segment may play an important role in the assembly of rEag1 subunits. As demonstrated by the published crystal structures of several prokaryotic and eukaryotic K^+ channels (31–34), in the closed conformation, the carboxyl termini of the S6 helices pack against each other in a bundle-crossing configuration like an inverted tepee. In Erg channels, results from molecular modeling with pore-binding drugs suggest that the carboxyl-terminal S6 region may also assume a similar bundle-crossing configuration (35, 36). It remains to be determined whether this tetramer packing model could indeed account for the intersubunit association mechanism of N470X and Q477X.

Nonetheless, the preceding inference does not exclude the possibility that the proximal carboxyl terminus (*e.g.* C-linker) may also be important for the formation of a functional rEag1 tetramer. Crystallographic study of the liganded C-linker-CNBD fragment of HCN2 channels suggests that most of the intersubunit contacts in the tetramer formed by the HCN2 fragments are mediated by helices of the C-linker (10, 37). Although cyclic nucleotides do not directly modulate Eag and Erg channels (38), homology modeling of the C-linker-CNBD region of Eag channels also supports a tetrametric conformation equivalent to that of the HCN2 channel (39). Together, these homology modeling results lead us to speculate the possibility that during early biogenesis, the initial step of tetramerization of rEag1 subunits may be mediated via the S6 segment and the proximal carboxyl terminus.

Our findings are not inconsistent with the previous report that CAD (or TCC domain) forms one of the subunit-subunit interaction sites in rEag1 tetramer (11, 12); rather they beg for a closer look into the role of this interaction in the biosynthesis of the channel. The formation of a tetrameric channel may require multiple intersubunit association sites, some acting as recognition motifs and others as stabilization motifs (25, 40). CAD, for instance, may contribute to the subfamily-specific assembly by deterring the formation of heterotetramers across Eag channel subfamilies (12). Other potential assembly-related functions of CAD may include a secondary recognition/stabilization site for the quaternary structure of rEag1 subunits. However, one cannot rule out the possibility that the importance of CAD is actually beyond the scope of tetramer formation. As mentioned above, we have noticed that the two rEag1 CAD-lacking truncation mutants yielded smaller maximal current amplitudes than those for WT. Similarly, truncations of carboxyl-terminal residues also generated several functional Erg mutants with reduced current amplitudes (16). Together these observations may reflect decreased functionality, increased protein degradation, or deficient trafficking of the truncation mutants. Interruption of CNBD or post-CNBD regions has been shown to disrupt Erg and HCN channel trafficking to the plasma membrane without affecting tetramer formation (41, 42). Our biotinylation and protein glycosylation analyses also demonstrated that progressive truncations of the carboxyl terminus result in aggravating disruptions of membrane trafficking and glycosylation of rEag1 proteins. More detailed investigation will thus be required in the future to address the possibility that the significance of CAD-mediated interaction may instead be related to protein folding and/or membrane trafficking. Finally, the three functional truncation mutants displayed a right-shifted steady-state activation curve, as well as a notable acceleration of the deactivation kinetics, implying that the distal end of carboxyl terminus may potentially modulate the gating of rEag1 channels.

In summary, our study provides evidence indicating that the S6 segment and the proximal carboxyl terminus may constitute the principal subunit recognition site for the assembly of rEag1 channels. We conclude that CAD as well as the distal end of the carboxyl terminus are not required for tetramer formation but may instead be important for ensuring proper protein biosynthesis.

Acknowledgment—We thank Dr. Chih-Yung Tang for technical guidance and critically reading the manuscript.

REFERENCES

1. Hille, B. (2001) *Ion Channels of Excitable Membranes*, pp. 131–167, Sinauer Associates, Inc., Sunderland, MA
2. MacKinnon, R. (1991) *Nature* **350,** 232–235
3. Li, M., Jan, Y. N., and Jan, L. Y. (1992) *Science* **257,** 1225–1230
4. Shen, N. V., Chen, X., Boyer, M. M., and Pfaffinger, P. J. (1993) *Neuron* **11,** 67–76
5. Shen, N. V., and Pfaffinger, P. J. (1995) *Neuron* **14,** 625–633
6. Schmitt, N., Schwarz, M., Peretz, A., Abitbol, I., Attali, B., and Pongs, O. (2000) *EMBO J.* **19,** 332–340
7. Maljevic, S., Lerche, C., Seebohm, G., Alekov, A. K., Busch, A. E., and Lerche, H. (2003) *J. Physiol.* **548,** 353–360
8. Schwake, M., Jentsch, T. J., and Friedrich, T. (2003) *EMBO Rep.* **4,** 76–81
9. Warmke, J. W., and Ganetzky, B. (1994) *Proc. Natl. Acad. Sci. U.S.A.* **91,** 3438–3442
10. Zagotta, W. N., Olivier, N. B., Black, K. D., Young, E. C., Olson, R., and Gouaux, E. (2003) *Nature* **425,** 200–205
11. Ludwig, J., Owen, D., and Pongs, O. (1997) *EMBO J.* **16,** 6337–6345
12. Jenke, M., Sánchez, A., Monje, F., Stühmer, W., Weseloh, R. M., and Pardo, L. A. (2003) *EMBO J.* **22,** 395–403
13. Daram, P., Urbach, S., Gaymard, F., Sentenac, H., and Chérel, I. (1997) *EMBO J.* **16,** 3455–3463
14. Dreyer, I., Porée, F., Schneider, A., Mittelstädt, J., Bertl, A., Sentenac, H., Thibaud, J. B., and Mueller-Roeber, B. (2004) *Biophys. J.* **87,** 858–872
15. Zhong, H., Molday, L. L., Molday, R. S., and Yau, K. W. (2002) *Nature* **420,** 193–198
16. Aydar, E., and Palmer, C. (2001) *J. Physiol.* **534,** 1–14
17. Li, X., Xu, J., and Li, M. (1997) *J. Biol. Chem.* **272,** 705–708
18. Phartiyal, P., Jones, E. M., and Robertson, G. A. (2007) *J. Biol. Chem.* **282,** 9874–9882
19. Flagg, T. P., Tate, M., Merot, J., and Welling, P. A. (1999) *J. Gen. Physiol.* **114,** 685–700
20. Craven, K. B., and Zagotta, W. N. (2006) *Annu. Rev. Physiol.* **68,** 375–401
21. Ludwig, J., Terlau, H., Wunder, F., Brüggemann, A., Pardo, L. A., Marquardt, A., Stühmer, W., and Pongs, O. (1994) *EMBO J.* **13,** 4451–4458
22. Tang, C. Y., Bezanilla, F., and Papazian, D. M. (2000) *J. Gen. Physiol.* **115,** 319–338
23. Robertson, G. A., Warmke, J. M., and Ganetzky, B. (1996) *Neuropharmacology* **35,** 841–850
24. Ribera, A. B. (1996) *J. Neurosci.* **16,** 1123–1130
25. Tu, L., Santarelli, V., Sheng, Z., Skach, W., Pain, D., and Deutsch, C. (1996) *J. Biol. Chem.* **271,** 18904–18911
26. Denning, G. M., Anderson, M. P., Amara, J. F., Marshall, J., Smith, A. E., and Welsh, M. J. (1992) *Nature* **358,** 761–764
27. Napp, J., Monje, F., Stühmer, W., and Pardo, L. A. (2005) *J. Biol. Chem.* **280,** 29506–29512
28. Lu, J., Robinson, J. M., Edwards, D., and Deutsch, C. (2001) *Biochemistry*

40, 10934–10946
29. Zerangue, N., Jan, Y. N., and Jan, L. Y. (2000) *Proc. Natl. Acad. Sci. U.S.A.* **97,** 3591–3595
30. Tu, L., Santarelli, V., and Deutsch, C. (1995) *Biophys. J.* **68,** 147–156
31. Jiang, Y., Lee, A., Chen, J., Cadene, M., Chait, B. T., and MacKinnon, R. (2002) *Nature* **417,** 523–526
32. Doyle, D. A., Morais Cabral, J., Pfuetzner, R. A., Kuo, A., Gulbis, J. M., Cohen, S. L., Chait, B. T., and MacKinnon, R. (1998) *Science* **280,** 69–77
33. Long, S. B., Campbell, E. B., and Mackinnon, R. (2005) *Science* **309,** 897–903
34. Kuo, A., Gulbis, J. M., Antcliff, J. F., Rahman, T., Lowe, E. D., Zimmer, J., Cuthbertson, J., Ashcroft, F. M., Ezaki, T., and Doyle, D. A. (2003) *Science* **300,** 1922–1926
35. Mitcheson, J. S., Chen, J., Lin, M., Culberson, C., and Sanguinetti, M. C. (2000) *Proc. Natl. Acad. Sci. U.S.A.* **97,** 12329–12333
36. Fernandez, D., Ghanta, A., Kauffman, G. W., and Sanguinetti, M. C. (2004) *J. Biol. Chem.* **279,** 10120–10127
37. Craven, K. B., and Zagotta, W. N. (2004) *J. Gen. Physiol.* **124,** 663–677
38. Brelidze, T. I., Carlson, A. E., and Zagotta, W. N. (2009) *J. Biol. Chem.* **284,** 27989–27997
39. Brelidze, T. I., Carlson, A. E., Davies, D. R., Stewart, L. J., and Zagotta, W. N. (2010) *PLoS One* **5,** e12523
40. Koster, J. C., Bentle, K. A., Nichols, C. G., and Ho, K. (1998) *Biophys. J.* **74,** 1821–1829
41. Akhavan, A., Atanasiu, R., Noguchi, T., Han, W., Holder, N., and Shrier, A. (2005) *J. Cell Sci.* **118,** 2803–2812
42. Akhavan, A., Atanasiu, R., and Shrier, A. (2003) *J. Biol. Chem.* **278,** 40105–40112